

*Supporting information for:*

**Modeling urban pollutant transport at multi-resolutions:**

**Impacts of turbulent mixing**

Zining Yang<sup>1</sup>, Qiuyan Du<sup>1</sup>, Qike Yang<sup>1</sup>, Chun Zhao<sup>1,2,3\*</sup>, Gudongze Li<sup>1</sup>, Zihan Xia<sup>1</sup>,  
Mingyue Xu<sup>1</sup>, Renmin Yuan<sup>1</sup>, Yubin Li<sup>4</sup>, Kaihui Xia<sup>1</sup>, Jun Gu<sup>1</sup>, and Jiawang Feng<sup>1</sup>

<sup>1</sup>Deep Space Exploration Laboratory/School of Earth and Space Sciences/CMA-USTC Laboratory of Fengyun Remote Sensing/State Key Laboratory of Fire Science/Institute of Advanced Interdisciplinary Research on High-Performance Computing Systems and Software, University of Science and Technology of China, Hefei, China

<sup>2</sup>Laoshan Laboratory, Qingdao, China

<sup>3</sup>CAS Center for Excellence in Comparative Planetology, University of Science and Technology of China, Hefei, China.

<sup>4</sup>School of Atmospheric Physics, Nanjing University of Information Science and Technology, Nanjing, China

\*Corresponding author: Chun Zhao (chunzhao@ustc.edu.cn)

## **Contents of this file**

Text S1: The process of grid refinement in this study.

Table S1: Description of land cover data classifications.

Figure S1: Three nested WRF-Chem domains.

Figure S2: Conceptual subdivision in this study.

Figure S3: The spatial distributions of BC emissions across multi-resolutions.

Figure S4: The spatial distributions of dry deposition velocity across multi-resolutions.

Figure S5: The spatial distributions of BC surface concentration differences between high- and low-resolutions.

Figure S6: The spatial distributions of BC surface concentration differences between the two higher-resolutions.

Figure S7: The spatial distributions of PBL mixing coefficient differences between high- and low-resolutions.

Figure S8: The spatial distributions of PBL mixing coefficient differences between the two higher-resolutions.

Figure S9: The latitude-pressure cross section of BC concentrations and wind flux across multi-resolutions along the USTC site.

Figure S10: The spatial distributions of friction velocity differences between high- and low-resolutions.

Figure S11: The spatial distributions of BC column concentration differences between high- and low-resolutions.

Figure S12: The spatial distributions of BC column concentration differences between the two higher-resolutions.

**Text S1. The process of grid refinement in this study.**

Due to the disparate grid sizes of the three resolution simulations impeding direct calculation of spatial distribution differences, we employ a grid refinement method to upscale the low-resolution grids to match the high-resolution grid cells. The grid refinement process involves dividing the cells in the original coarse grid into finer cells. Specifically, the 25 km grids are divided into 25 x 25 small grids and the 5 km grids are divided into 5 x 5 small grids. This approach ensures that the grid resolution of all three simulations is identical while preserving spatial details, thus allowing us to quantify the differences between the 25 km resolution simulations and the two higher-resolution simulations.

**Table S1.** Description of land cover data classifications

<b>Number</b>	<b>Description</b>
1	Urban
2	Dryland cropland/pasture
3	Irrigated cropland/pasture
4	Mixed Dryland/Irrigated Cropland
5	Cropland/Grassland Mosaic
6	Cropland/Woodland Mosaic
7	Grassland
8	Shrubland
9	Mixed Shrubland/Grassland
10	Savanna
11	Deciduous Broadleaf Forest
12	Deciduous Needleleaf Forest
13	Evergreen Broadleaf Forest
14	Evergreen Needleleaf Forest
15	Mixed Forest
16	Water
17	Herbaceous Wetland
18	Wooded Wetland
19	Barren or Sparsely Vegetated
20	Herbaceous Tundra
21	Wooded Tundra
22	Mixed Tundra
23	Bare Ground Tundra
24	Snow or Ice

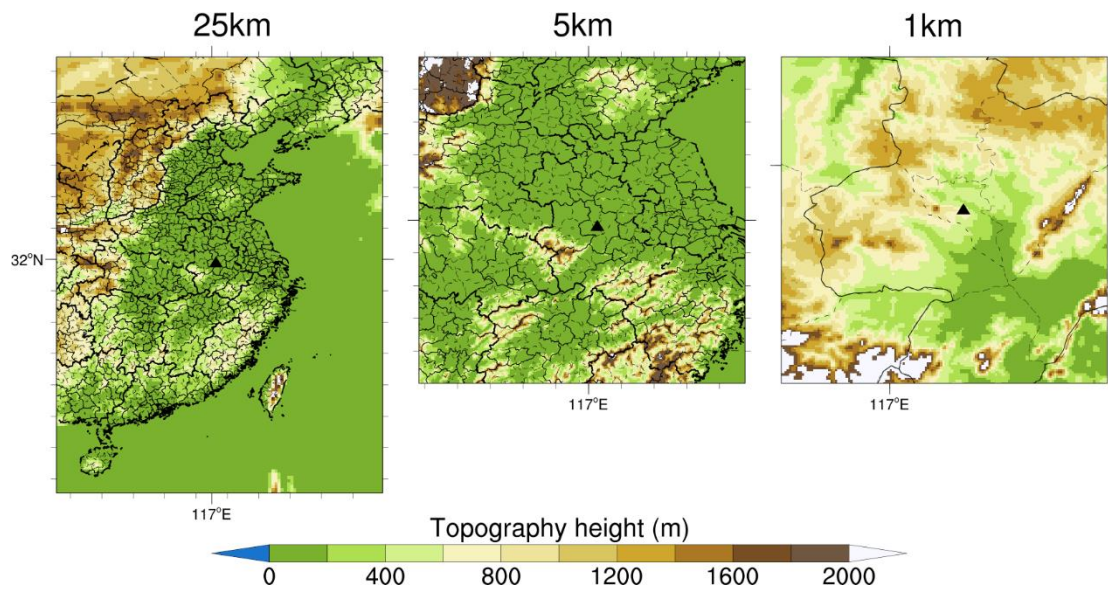


**Figure S1.** The three domains in the WRF-Chem simulations and the terrain height (m) of each domain. Domain one (D1) has a horizontal grid spacing of 25 km, domain 2 (D2) 5 km, and domain 3 (D3) 1 km. The solid black triangle indicates the location of the USTC site.

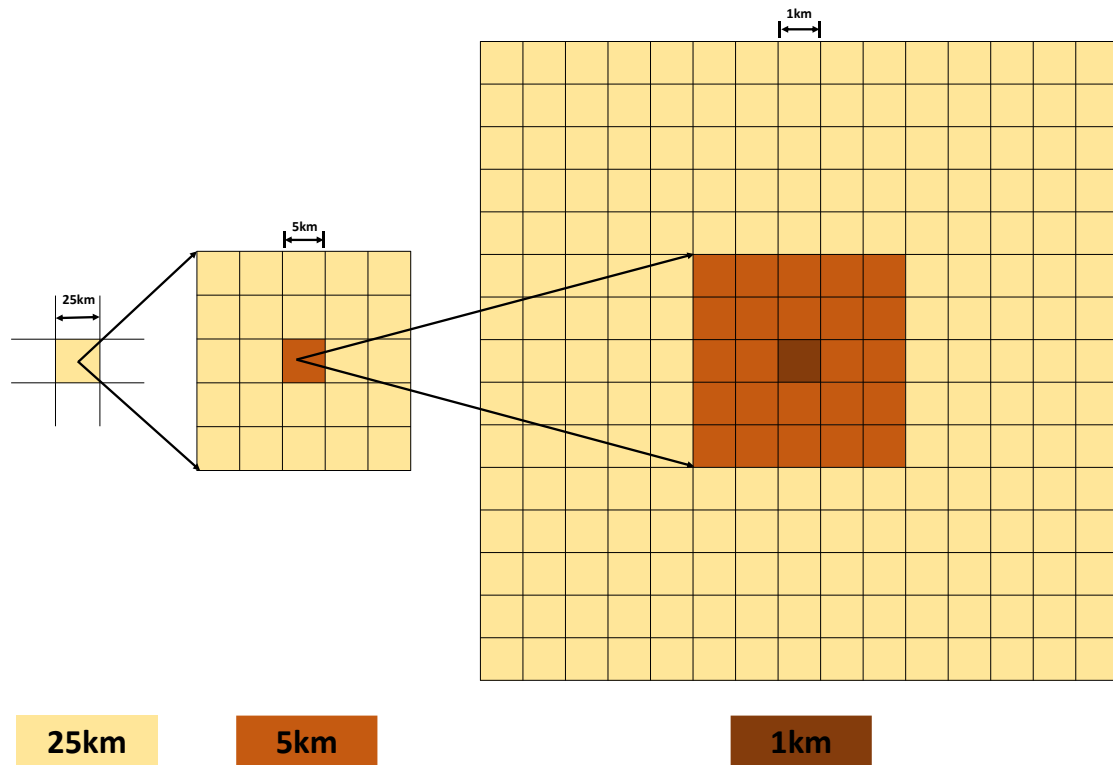


**Figure S2.** Conceptual subdivision of a coarse grid cell from the 25-km grid into smaller grid points for the finer grids. Each 25-km grid cell is subdivided into 25 5-km grid cells. Each of the 5-km grid cells are further refined into 25 1-km grid cells for a total of 625 1-km grid cells per 25-km cell. The solid black triangle indicates the location of the USTC site.

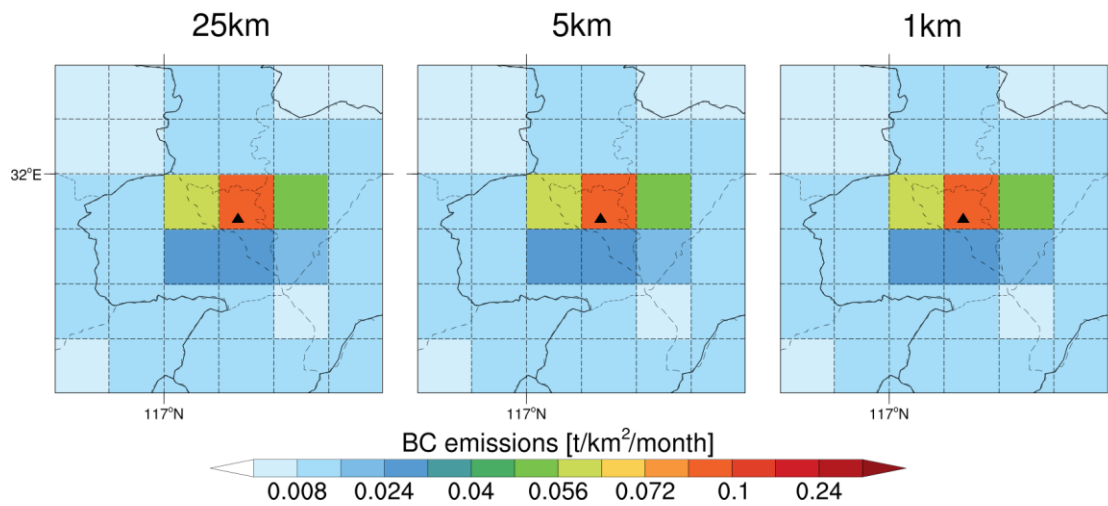


**Figure S3.** Spatial distribution of BC emissions in the study area for 25-km (left), 5-km (middle), and 1-km (right) resolution simulations, respectively. The solid black triangle indicates the location of the USTC site.



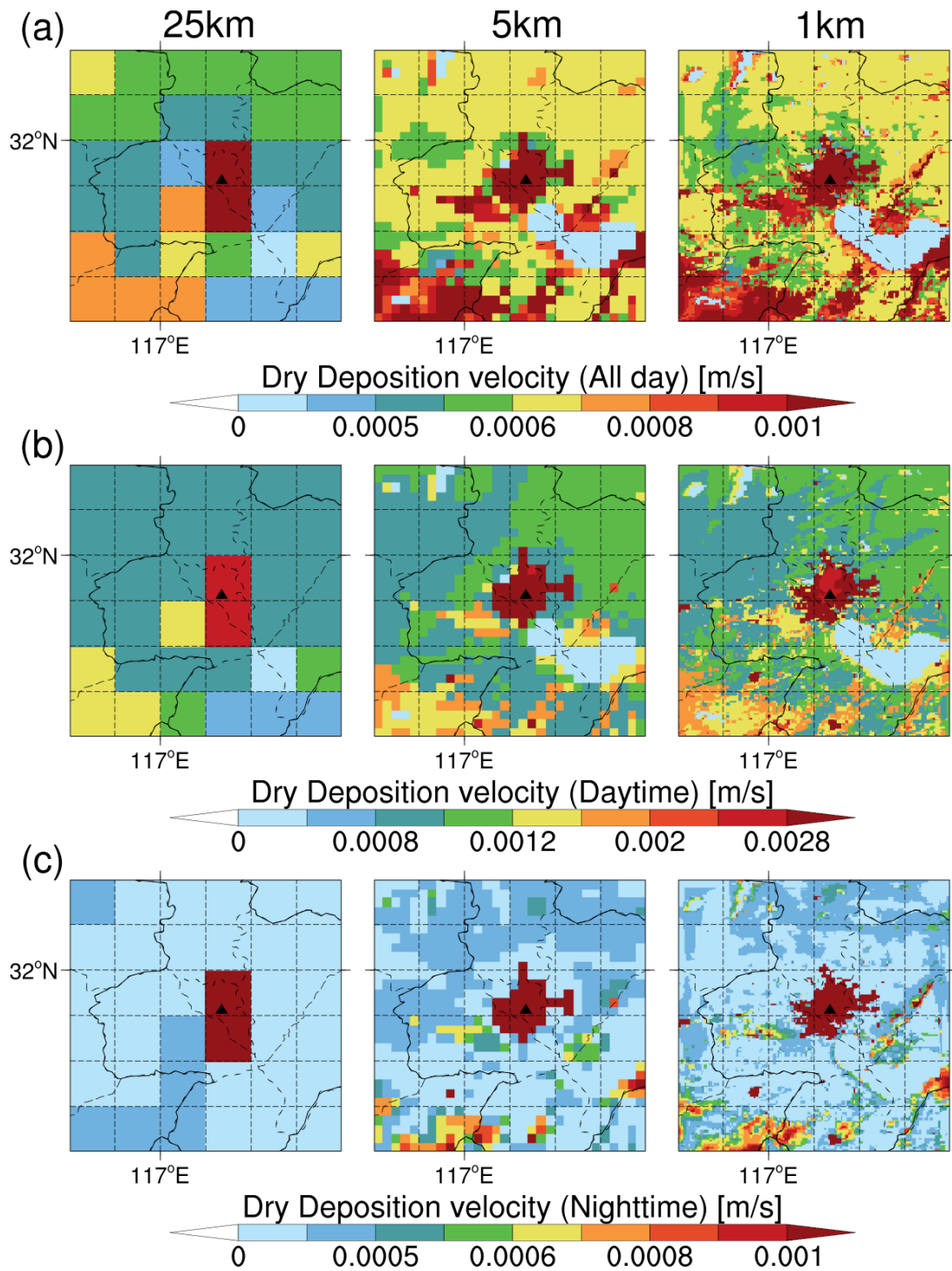


**Figure S4.** Spatial distribution of the dry deposition velocity in the study area for 25-km (left), 5-km (middle), and 1-km (right) resolution simulations of the whole day (top), the daytime (middle), and the nighttime (bottom), respectively. The solid black triangle indicates the location of the USTC site.

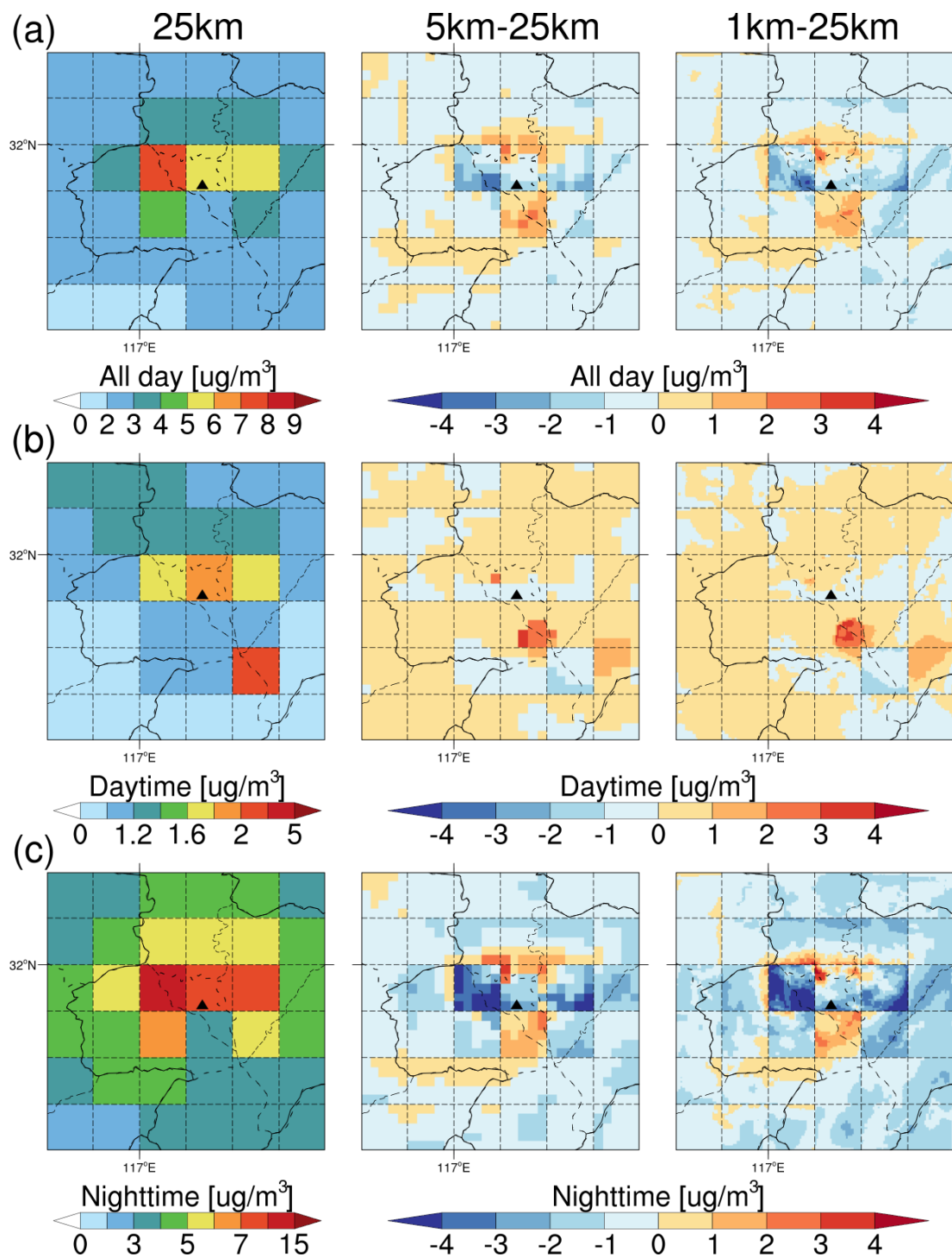


**Figure S5.** Spatial distribution of the BC surface concentration in the study area for 25-km resolution (left), the difference between 25-km and 5-km resolutions (middle), and the difference between 25-km and 1-km (right) resolutions of the whole day (top), the daytime (middle), and the nighttime (bottom), respectively. The solid black triangle indicates the location of the USTC site.

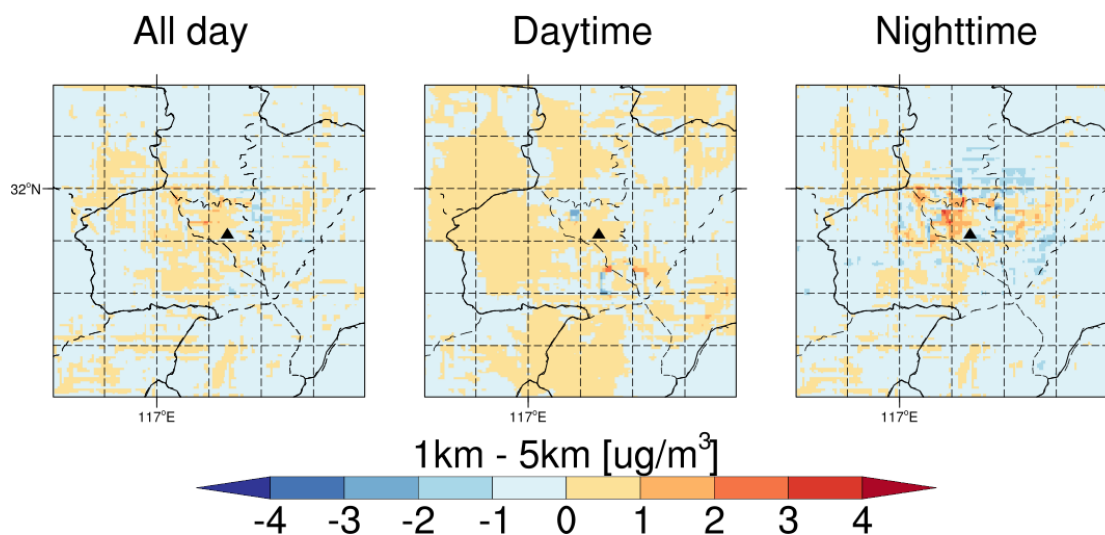


**Figure S6.** Spatial distribution of the differences in BC surface concentrations between 1-km and 5-km resolutions in the study area of the whole day (left), the daytime (middle), and the nighttime (right), respectively. The solid black triangle indicates the location of the USTC site.

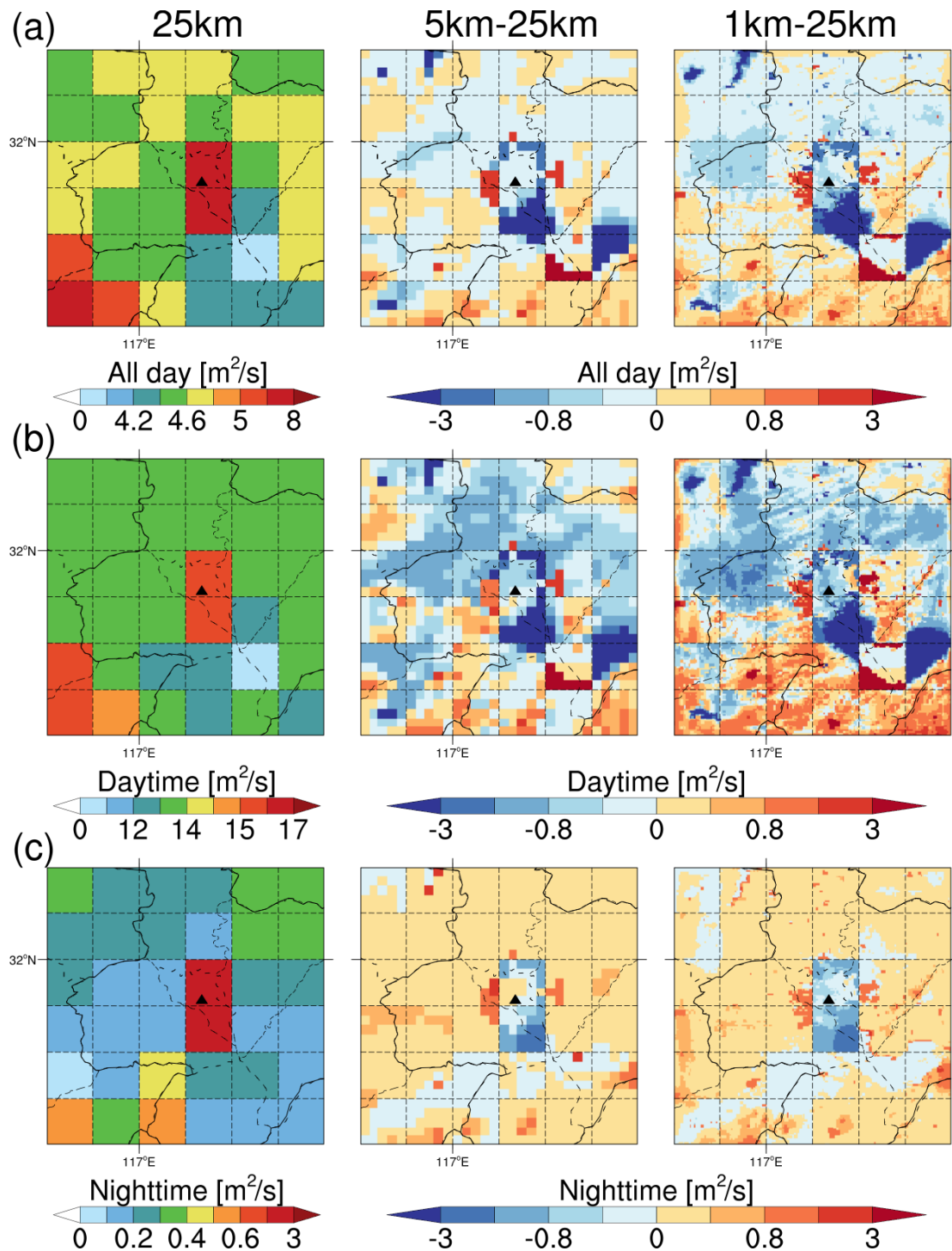


**Figure S7.** Spatial distribution of PBL mixing coefficients in the study area for 25-km resolution (left), the difference between 25-km and 5-km resolutions (middle), and the difference between 25-km and 1-km (right) resolutions of the whole day (top), the daytime (middle), and the nighttime (bottom), respectively. The solid black triangle indicates the location of the USTC site.

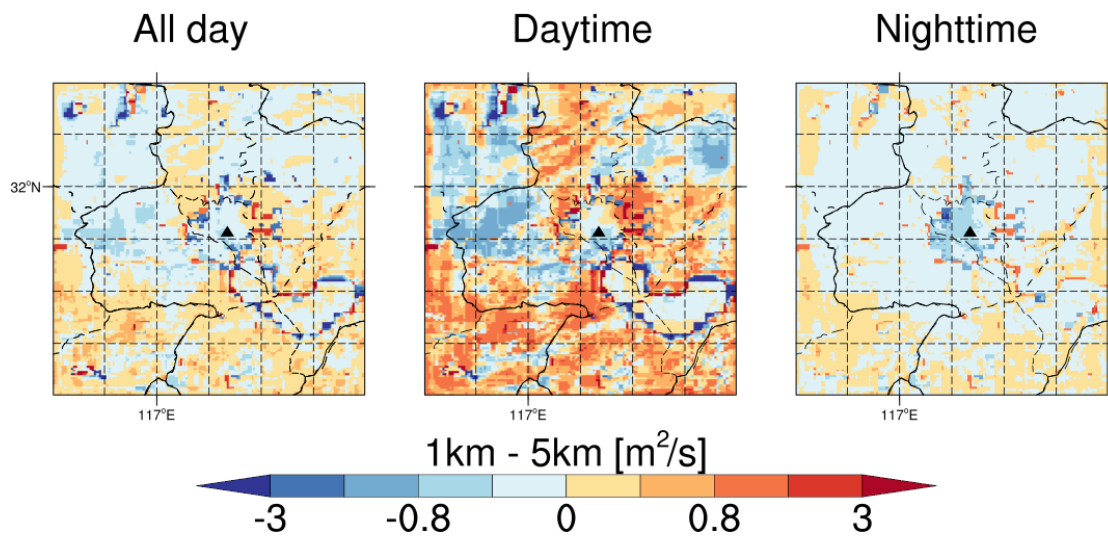


**Figure S8.** Spatial distribution of the differences in PBL mixing coefficients between 1-km and 5-km resolutions in the study area of the whole day (left), the daytime (middle), and the nighttime (right), respectively. The solid black triangle indicates the location of the USTC site.

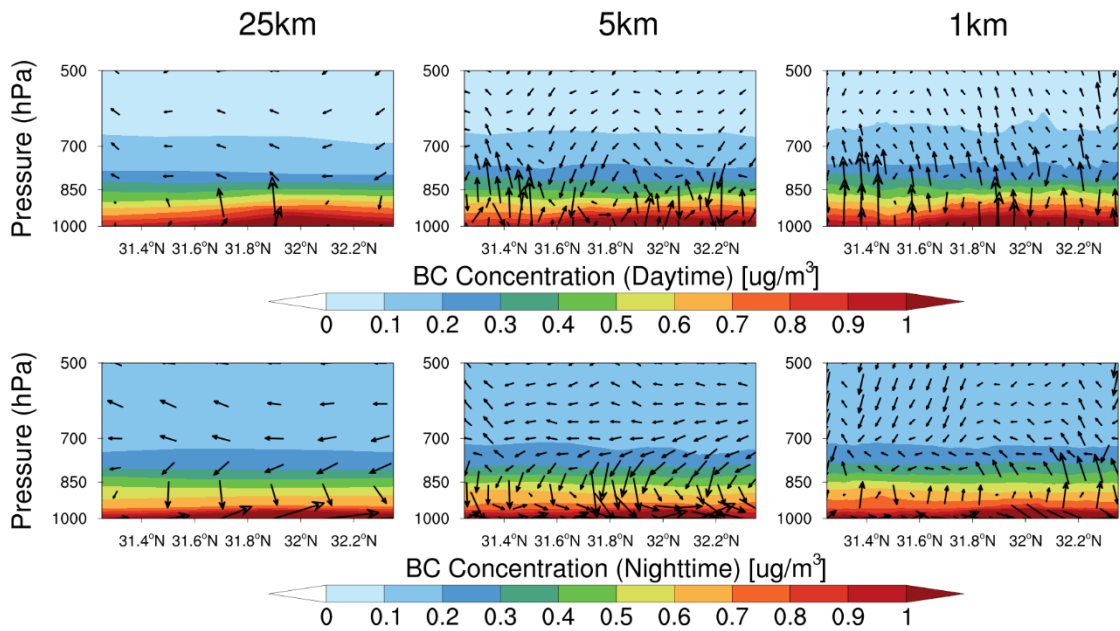


**Figure S9.** The latitude-pressure cross section of BC concentrations and wind speed flux along the USTC site for 25-km (left), 5-km (middle), and 1-km (right) resolution simulations of the daytime (top), and the nighttime (bottom), respectively. Vector arrows are the combination of wind speed fluxes  $v$  and  $w$ , with the vertical wind speed flux being multiplied by 100 for visibility. The shaded contours represent BC concentrations at each pressure level.

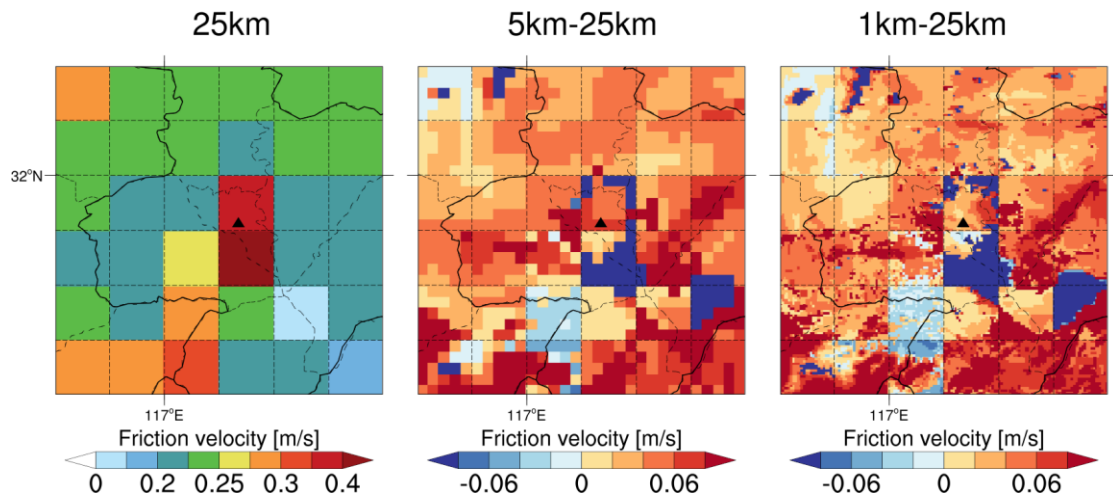


**Figure S10.** Spatial distribution of the friction velocity in the study area for 25-km resolution (left), the difference between 25-km and 5-km resolutions (middle), and the difference between 25-km and 1-km resolutions (right) simulations of the whole day, respectively. The solid black triangle indicates the location of the USTC site.

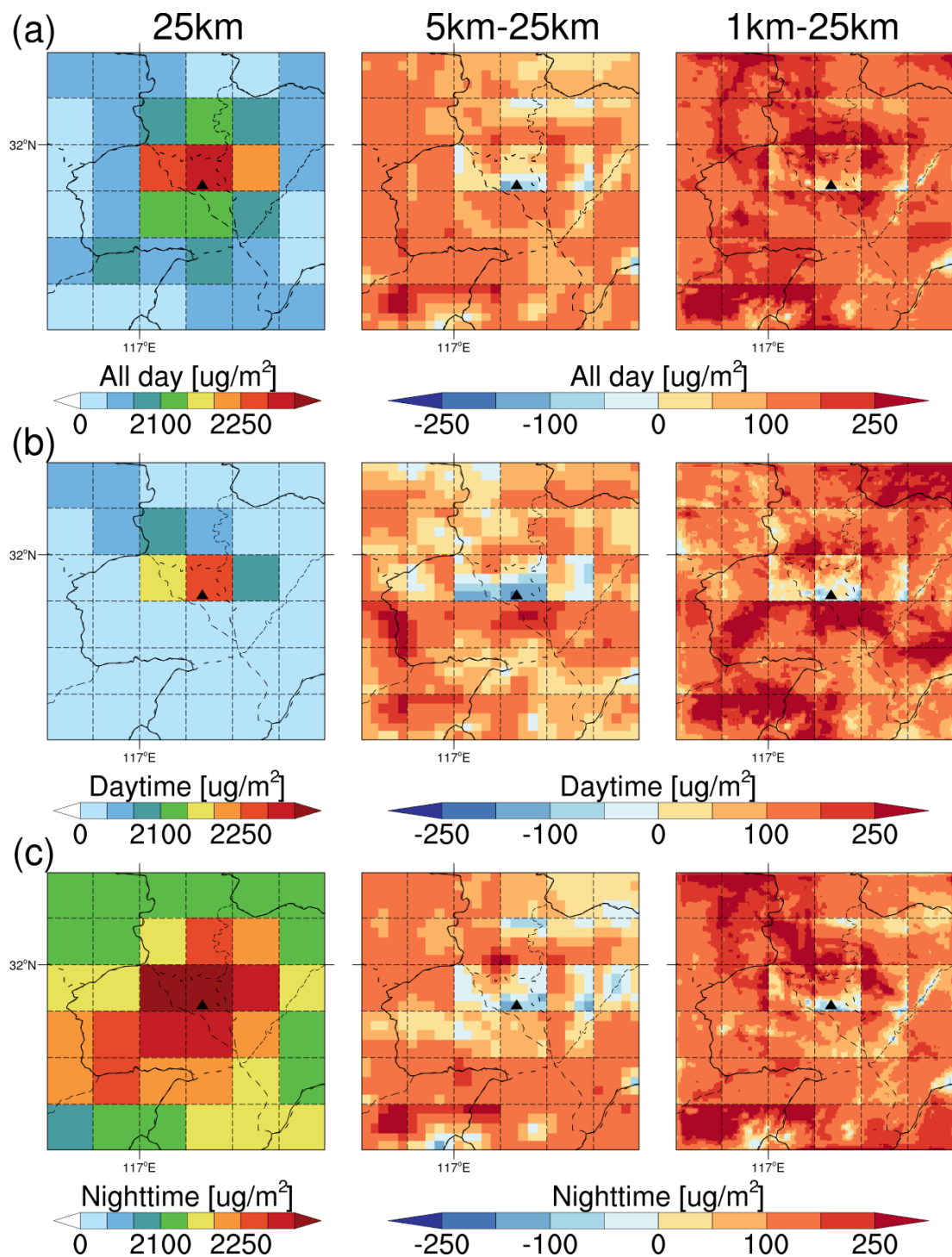


**Figure S11.** Spatial distribution of the BC column concentration in the study area for 25-km resolution (left), the difference between 25-km and 5-km resolutions (middle), and the difference between 25-km and 1-km (right) resolutions of the whole day (top), the daytime (middle), and the nighttime (bottom), respectively. The solid black triangle indicates the location of the USTC site.



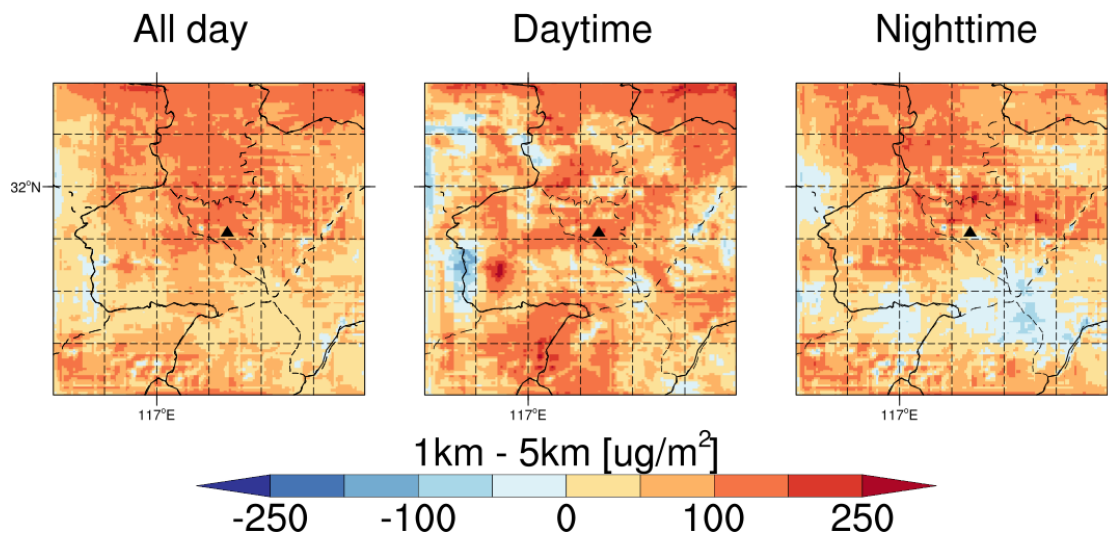


**Figure S12.** Spatial distribution of the differences in BC column concentrations between 1-km and 5-km resolutions in the study area of the whole day (left), the daytime (middle), and the nighttime (right), respectively. The solid black triangle indicates the location of the USTC site.